ELSEVIER

Journal of Nuclear Materials 294 (2001) 8–12

journal of nuclear materials

www.elsevier.nl/locate/jnucmat

Phase equilibria in the UO_2–PuO_2 system under a temperature gradient

Heiko Kleykamp *

Forschungszentrum Karlsruhe, Institut für Materialforschung I, Postfach 3640, Karlsruhe 76021, Germany

Abstract

The phase behaviour of $U_{0.80}Pu_{0.20}O_{1.95}$ was investigated under a steady-state temperature gradient between the solidus and liquidus by a short-time power-to-melt irradiation experiment. The radial U, Pu, Am and O profiles in the fuel pin after redistribution were measured by X-ray microanalysis. During irradiation, an inner fuel melt forms which is separated from the outer solid only by one concentric liquid–solid-phase boundary. The UO_2 concentration increases to 85% and the PuO_2 concentration decreases to 15% on the solid side of the interface. Opposite gradients occur on the liquid side of the interface. The concentration discontinuity is a consequence of the necessary equality of the chemical potentials of UO_2 and PuO_2 on both sides of the phase boundary which corresponds to a 2750°C isotherm. The radial oxygen profile results in an O/(U + Pu) ratio of 2.00 at the fuel surface and 1.92 at the central void of the fuel. The redistribution is caused by the thermal diffusion of oxygen vacancies in the lattice along the temperature gradient. This process is quantified by the heat of transport Q_v^* which ranges between −10 kJ/mol at the central void and about −230 kJ/mol near the fuel surface.

1. Introduction

UO_2 and PuO_2 are completely miscible in the solid and the liquid. When a $U_{0.8}Pu_{0.2}O_2$ solid solution is heated to a temperature between the solidus (2730°C [1]) and the liquidus (2780°C [1]), coexisting solid and liquid phases are formed. The liquid is richer in PuO_2 than the solid. A single-phase melt exists above the liquidus. These temperatures are insignificantly lower in hypostoichiometric $U_{0.8}Pu_{0.2}O_{1.95}$ with a temperature difference of about −20 degrees [2]. When $U_{1-x}Pu_xO_2$ is rapidly heated above the solidus and a steady-state temperature gradient is attained in the fuel between the melting temperatures of UO_2 and PuO_2, first of all a solid–liquid two-phase region is formed containing UO_2 rich solid particles in a PuO_2 rich melt. However, the position of the solid particles is unstable under the temperature gradient. Their UO_2 richer hot sides are dissolved in the melt and UO_2 resolidifies on their cold sides in a manner that the entire particles move to the solid-phase boundary which becomes richer in UO_2. The two-phase field disappears immediately. The discontinuous UO_2 and PuO_2 concentrations fulfil the conditions of identical chemical potentials of UO_2 and PuO_2 which must be equal at the phase boundary between the solid and the liquid phase at about 2750°C. The concentrations are 84% UO_2 in the solid and 75% UO_2 in the liquid according to the phase diagram of the UO_2–PuO_2 system [1]. The course of the PuO_2 concentration is complementary. An assessment of the spatial extent of the concentration gradient is more difficult. The solid interface near region is broader than the liquid one due to UO_2 diffusion to the solid side of the interphase. The model of the discontinuous UO_2 and PuO_2 concentrations is qualitatively exemplified in Fig. 1. This phenomenon may be illustrated by the analogue of a pore transport in irradiated fuel under a temperature gradient. The pores move to higher temperatures by fuel evaporation from the hot side of the pores and recondensation on their cold side. The moving mass is part of the fuel matrix. In the case of a solid particle in a melt, the moving mass is part of the particle and is transported against the temperature gradient.

* Tel.: +49-7247 82 2888; fax: +49-7247 82 4567.

E-mail address: heiko.kleykamp@imf.fzk.de (H. Kleykamp).

0022-3115/01/$ - see front matter
PII: S0022-3115(01)00441-X

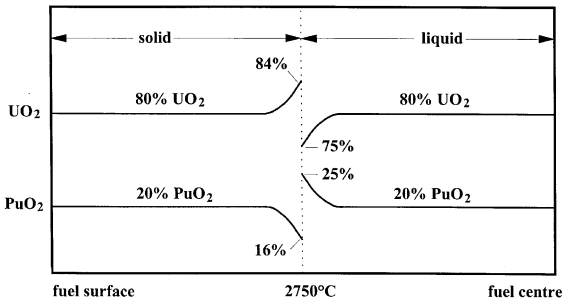

Fig. 1. Model of the segregation of $U_{0.80}Pu_{0.20}O_2$ in a steady-state temperature gradient at the solid–liquid interface.

It is well known from experiments and modelling that the UO_2–PuO_2 solid solution which is exposed to a thermal gradient segregates with respect to the components. The difference of their lattice energies and their temperature dependence results in a matter flow moving along the temperature gradients in positive or negative directions [3]. Two segregation phenomena are observed, which generate concentration gradients, the U/Pu redistribution in the cation sublattice and the O/(U + Pu) redistribution enabled by intrinsic defects in the anion sublattice. The macroscopic U/Pu redistribution phenomena were demonstrated in irradiated UO_2–PuO_2 fuel pins by post-irradiation examinations. Three models predict semi-quantitatively the radial O/(U + Pu) redistribution in fuel pins under the influence of a temperature gradient. They are founded on gas equilibria [4], on the oxygen diffusion via the solid and gaseous phases [5] and on thermal diffusion of oxygen vacancies or interstitials as a typical long-term effect [6].

Several indirect experimental methods have been applied to quantify radial oxygen concentration gradients in irradiated mixed oxide fuel pins. Early X-ray microanalysis of oxygen in irradiated oxide fuel evidenced a radial oxygen concentration gradient. However, the error bars of the measured O Kα intensities were so high that there was no sufficient support for oxygen redistribution [7]. Other investigators used the lattice parameters measured by X-ray diffraction on micro-drilled $(U,Pu)O_{2-x}$ samples and evaluated therefrom the oxygen concentration as a function of the fuel radius [8,9]. The molybdenum fraction in the metallic Mo–Tc–Ru–Rh–Pd precipitates and the MoO_2 fraction in the fuel matrix and in the ceramic Ba(U, Pu, Zr, RE, Mo)O_3 precipitates, respectively, were measured by X-ray microanalysis in $(U,Pu)O_{2-x}$ fuel. The oxygen potential was evaluated from the $Mo + O_2 = MoO_2$ equilibrium in these phases which allows to calculate the oxygen concentration as a function of the fuel radius [10,11]. Finally, electrochemical methods using solid electrolyte microprobes were applied to measure directly the oxygen potential as a function of the relative fuel

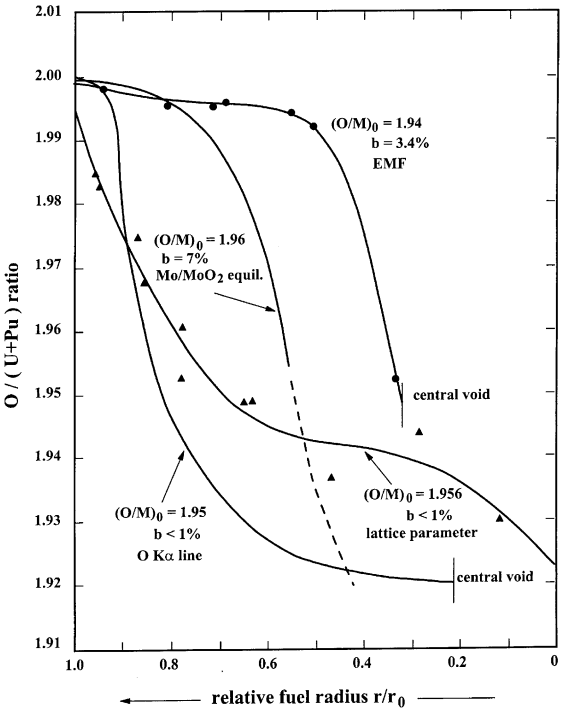

Fig. 2. Oxygen redistribution in irradiated $(U,Pu)O_{2-x}$ pins as a function of the relative fuel radius by measurements of the chemical potential of oxygen [13], of the Mo/MoO_2 concentration in the fission product precipitates [11], of the lattice parameter of the fuel [9] and of the oxygen concentration in the fuel by X-ray microanalysis, this study.

radius of $(U,Pu)O_{2-x}$. The oxygen concentration was calculated therefrom [12,13]. Selected examples are illustrated in Fig. 2 by plotting the local O/M ratio, M = U + Pu, as a function of the relative fuel radius. The initial $(O/M)_0$ ratios and the burnups b are different in these examples, the O/M ratios of the fuels increase during the irradiations.

2. Experimental

2.1. Irradiation experiment

An irradiated austenitic steel cladded fuel pin is now available with solid pellets and a very high fuel density of 97.4% of theoretical density. The specified composition of the fuel fabricated by the OCOM method is $U_{0.80}Pu_{0.20}O_{1.95}$ with the enrichments 83% U-235/U-total and 82% Pu-fiss/Pu-total. The O/M ratio was measured to be 1.949 [14]. A so-called power-to-melt experiment POTOM-3 was carried out in the high-flux reactor in Petten. The steady-state pre-irradiation

period was 89 h with a maximum linear heat rating of $\chi = 51$ kW/m. A ramp up to $\chi = 67$ kW/m within 100 s and a 170 s steady-state irradiation followed. A fast shut-down terminated the transient irradiation. A steady-state follow-on irradiation took 436 h with $\chi = 41$ kW/m [14]. The fuel temperature increased in the transient irradiation period beyond the fuel melting point in the inner pin region. As the burnup was low (<1%) the generated fission products did not influence the quantitative oxygen concentration measurement.

2.2. X-ray microanalysis

The quantitative U, Pu, Am and O analysis of the fuel with the nominal composition $U_{0.8}Pu_{0.2}O_{1.95}$ was performed with the γ-shielded X-ray microanalyser JRXA-50 of JEOL Ltd. (1974 model) of which the complete electron optics inclusive the electron optical column was replaced by the scanning electron microscope JSM 6400 (1990 model). Furthermore, the worn-out specimen stage was exchanged and a modern light-optical microscope with a CCD camera was installed. The following parameters were selected for the analysis: working voltage, 15 kV; beam current for point analysis, 100 nA; counting time for peak and for background left and right from the peak, 200 s. A carbon contamination on the sample surface did not appear by use of a turbomolecular pump. The vacuum in the lower range of the cathode region was about 3×10^{-9} bar. Uranium and americium were analysed with the Mα lines using a PET diffracting crystal, plutonium with the Mβ line using a quartz 1011 diffracting crystal. A synthetic Ni–C multilayer device was utilised for the oxygen analysis. The $2d = 8.3$ nm lattice spacing is more favourable than the normally used lattice spacing $2d = 10$ nm of an ODPb diffracting crystal due to a longer distance between sample and crystal and therefore, due to the lower radioactive background. The oxygen analysis was made in the differential mode with 0.7 V level and 3.5 V window. A further improvement of the O Kα net count rate was attained by the increase of the counter tube voltage to 1780 V and the use of a special gas for the proportional counter. A $UO_{2.003}$ standard was used for the U and O analysis, a $PuO_{2.0}$ standard for the Pu analysis and a $U_{0.5}Am_{0.5}O_2$ standard for the Am analysis. A $\varphi\rho z$ correction procedure did not change the intensities by their conversion to mass concentrations because sample and standards were similar. The oxygen analysis of the sample gave typically 70, 000 net pulses P–B and 19, 000 background pulses B after 200 s measuring time, hence the counting statistics yields a double S.D. (95%) of the average value $2\varepsilon = \pm 0.94\%$ relative and a detection limit $c_{\min} = 0.065\%$ oxygen absolute.

3. Results

3.1. U/Pu redistribution

The etched light-optical microstructure and the complementary α-autoradiograph of an axial cut of pin No. 206 of the OCOM 3 experiment are illustrated in Fig. 3. A similar radial cut of pin No. 205 in the same axial pin position was investigated by X-ray microanalysis. Both microstructures are characterised by an axial–circular central void and a poorly defined transition from the equiaxed grain zone to the columnar grain zone. The α-autoradiograph unequivocally makes out a dark narrow concentric ring which points to the solid–liquid phase boundary that cannot be detected in the

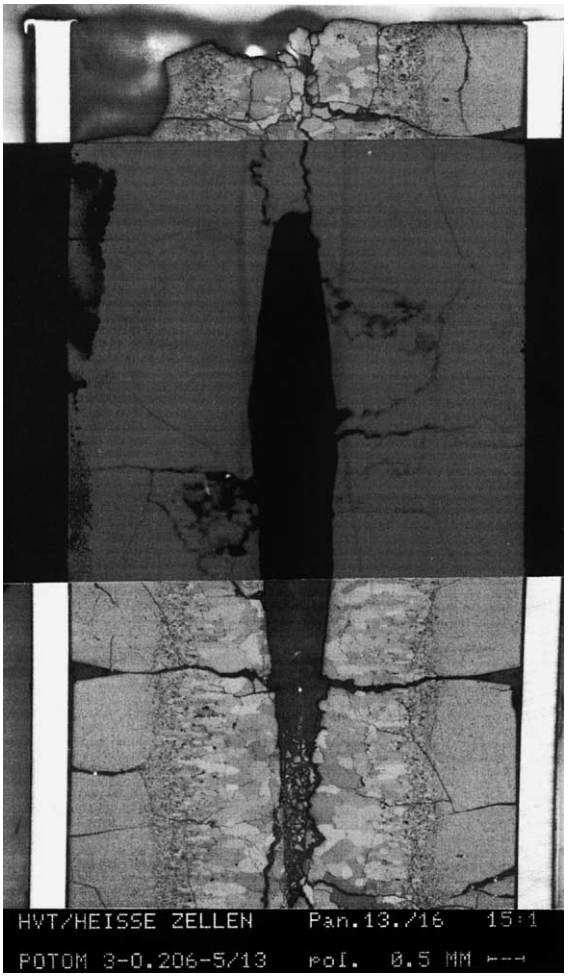

Fig. 3. Etched light-optical microstructure and α-autoradiograph of an axial cut of the power-to-melt experiment POTOM-3. The dark border in the autoradiograph is the PuO_2 depleted solid–liquid phase boundary of the fuel during the transient irradiation.

microstructure. The concentration profiles of U, Pu, Am and O were determined by step scans in 25 μm intervals as a function of the relative fuel radius r/r_0. The fuel section averaged concentrations are 79.4% UO_2, 19.2% PuO_2 and 0.43% AmO_2. The sum is 99.0%. The difference to 100% is due to the presence of the dissolved fission products which were generated by the 525 h steady-state irradiation before and after the transient period.

In order to confirm the model of the uranium–plutonium segregation in a solid solution under a temperature gradient, point analyses of U and Pu were made in 10 μm steps in the region of the solid–liquid interface. Discontinuities of the U and Pu profiles were observed on the solid side of the interface at the relative fuel radius $r/r_0 = 0.44$ yielding a concentration increase up to 85% UO_2 and a decrease down to 15% PuO_2. A concentration gradient is not visible on the liquid side of the interface. A high scatter of the Pu concentration was observed because the liquid state could not be frozen in. It decomposed into two solid solutions with different U/Pu ratios which could not homogenise during cooling, see Fig. 4. The measured UO_2 and PuO_2 concentrations on the solid side of the solid–liquid interface (Fig. 4) agree well with the predicted concentrations 84% UO_2 and 16% PuO_2. These values correspond to an interface temperature of 2750°C according to the phase diagram of the pseudo-binary UO_2–PuO_2 system [1]. A Pu enrichment up to 23% PuO_2 was observed at the central void which is caused by a preferential UO_2 evaporation from this fuel region.

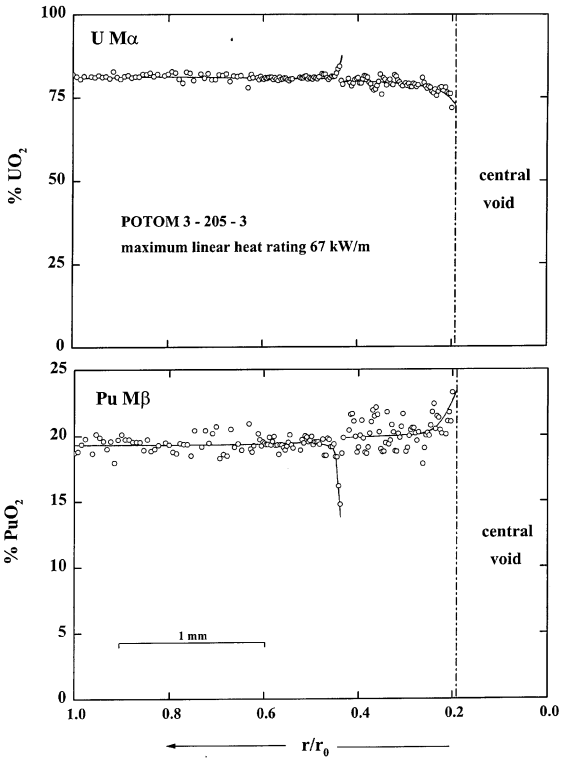

Fig. 4. UO_2 and PuO_2 concentration of the irradiated $U_{0.8}Pu_{0.2}O_{1.95}$ fuel pin as a function of the relative fuel radius r/r_0. The solid–liquid interface is located at $r/r_0 = 0.44$.

3.2. O/(U+Pu) redistribution

The oxygen net counts per second are plotted as a function of the relative fuel radius r/r_0 in Fig. 5. The fuel section averaged counts are 340 s^{-1} which are correlated with the initial O/(U + Pu) ratio 1.95 of the fuel. The right-hand ordinate calibration was made under the assumption of linearity between oxygen net count rate and oxygen mass concentration in the fuel. A discontinuity of the oxygen concentration at the melting boundary of the fuel was not observed. The O/(U + Pu) ratio is 2.00 at the fuel surface and becomes strongly hypostoichiometric, O/(U + Pu) = 1.92, with a nearly horizontal tangent at the central void. The oxygen concentration gradient in hypostoichiometric $(U,Pu)O_{2-x}$ under a temperature gradient is controlled by the oxygen vacancy flux in the direction of the temperature gradient (to higher temperatures). The oxygen profile can be quantified by the heat of transport of oxygen vacancies Q_v^* which is dependent on the local plutonium valency and the O/(U + Pu) ratio, respectively. According to Schumacher et al. [3,6] Q_v^* becomes about −140 kJ/mol at O/(U + Pu) = 2.00 and tends to zero at O/(U + Pu) ≈ 1.93.

The oxygen concentration profile in Fig. 5 was used to recalculate the heat of transport of oxygen vacancies in $U_{0.8}Pu_{0.2}O_{1.95}$. The fuel cross-section was divided into 17 concentric fuel rings. The local O/(U + Pu) ratio was correlated with the relative fuel radius $r/r_0 = \rho$ in each ring. A radial parabolic temperature profile was

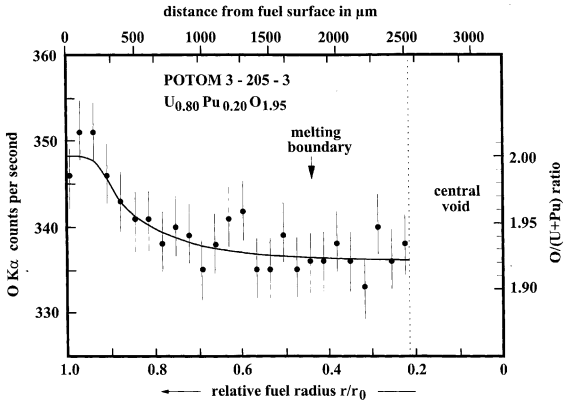

Fig. 5. Oxygen concentration of the irradiated $U_{0.80}Pu_{0.20}O_{1.95}$ fuel pin as a function of the relative fuel radius r/r_0.

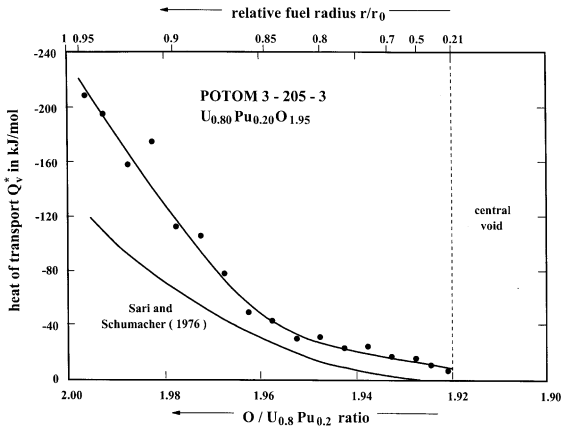

Fig. 6. Heat of transport of oxygen vacancies Q_v^* in irradiated $U_{0.80}Pu_{0.20}O_{1.95}$ fuel as a function of the local O/(U + Pu) ratio.

calculated under the following conditions: (1) vertex of the parabola at the central void, $\rho = 0.21$, (2) solid–liquid interface temperature $T = 2750$°C at $\rho = 0.44$, (3) estimated fuel surface temperature $T = 800$°C at $\rho = 1$. These parameters result in the temperature T (in °C) as a function of the relative fuel radius ρ:

$$T(\rho) = -3414\ (\rho - 0.21)^2 + 2931, \tag{1}$$

T_i' and T_k' are the temperatures (in K) within two adjacent concentric fuel rings and x_i and x_k are the deviations from stoichiometry $O/U_{0.8}Pu_{0.2} = 2 - x$ in the corresponding rings taken from Fig. 5. The heat of transport of oxygen vacancies Q_v^* can be calculated using the equation [6]

$$\frac{Q_v^* = R \ln x_i/x_k}{1/T_i' - 1/T_k'}. \tag{2}$$

The result is plotted as a function of the $O/U_{0.8}Pu_{0.2}$ ratio in Fig. 6. The heat of transport is strongly dependent on the fuel stoichiometry: $Q_v^* = -230$ kJ/mol for $O/U_{0.8}Pu_{0.2} = 2.00$ (plutonium valency 4) on the fuel surface and tends to zero at about $O/U_{0.8}Pu_{0.2} = 1.90$ (plutonium valency 3) at the central void. The trend is the same in the curve of Sari and Schumacher [6], see Fig. 6. The smaller absolute values of their pioneering work should be honourably mentioned in the background of restricted analytical techniques 25 years ago.

4. Conclusions

Uranium–plutonium oxide fuel pins steady-state irradiated up to the power-to-melt are characterised by an inner molten, stable fuel zone surrounded by an outer solid fuel skeleton. The UO_2 and PuO_2 concentrations at the liquid–solid interface are discontinuous in order to meet the requirements of equal chemical potentials of the components in the phases on both sides of the boundary. The measurements of the oxygen-to-metal redistribution in the temperature gradient of $U_{0.8}Pu_{0.2}O_{1.95}$ yield an O/M ratio of 1.92 at the central void. The oxygen concentration gradient becomes infinitely small in this fuel region. The heat of transport of the oxygen vacancies approaches zero at $O/U_{0.8}Pu_{0.2} = 1.90$.

Acknowledgements

The author gratefully acknowledges the fruitful discussions with Dr G. Schumacher, Forschungszentrum Karlsruhe.

References

[1] T. Philipponeau, Melting Point of U–Pu Mixed Oxide Fuels, Fast Reactor European Collaboration Data Sheet, 1990.
[2] E.A. Aitken, S.K. Evans, Report GEAP-5672, 1968.
[3] M. Bober, G. Schumacher, Adv. Nucl. Sci. Technol. 7 (1973) 121.
[4] M.H. Rand, T.L. Markin, in: Thermodyn. Nucl. Mater. 1967, Proceedings of the IAEA Symposium, Vienna, 1968, p. 637.
[5] M.G. Adamson, E.A. Aitken, S.K. Evans, J.H. Davies, in: Thermodyn. Nucl. Mater. 1974, Proceedings of the IAEA Symposium, Vienna, 1975, p. 73.
[6] C. Sari, G. Schumacher, J. Nucl. Mater. 61 (1976) 192.
[7] T.E. Lannin, R.C. Wolf, H.S. Rosenbaum, G.F. Melde, in: 6th National Conference on Electron Probe Analysis, Pittsburgh, Proceedings Symposium, 1971, p. 24A.
[8] U. Benedict, M. Coquerelle, J. de Bueger, C. Dufour, J. Nucl. Mater. 45 (1972) 217.
[9] M. Conte, J.P. Gatesoupe, M. Trotabas, J.C. Boivineau, G. Cosoli, in: Proceedings of the International Conference on Fast Breeder Reactor Fuel Performance, Monterey, CA, ANS, 1979, p. 301.
[10] I. Johnson, C.E. Johnson, C.E. Crouthamel, C.A. Seils, J. Nucl. Mater. 48 (1973) 21.
[11] H. Kleykamp, J. Nucl. Mater. 66 (1977) 292.
[12] F.T. Ewart, L. Manes, Hj. Matzke, C.M. Mari, F. Toci, R. Schreiber, J. Nucl. Mater. 81 (1979) 185.
[13] F.T. Ewart, K. Lassmann, Hj. Matzke, L. Manes, A. Saunders, J. Nucl. Mater. 124 (1984) 44.
[14] D. Freund, Die Analyse des Brennstoffschmelzexperiments POTOM3 – Abschlussbericht, PSF-Ber. 3208, 1995.